Electronic Supplementary Information (ESI)

Kinetic Investigation on the Chemoselective Hydrogenation of α,β-Unsaturated Carbonyl Compounds Catalysed by Ni(0) Nanoparticles

Laíze Zaramello[a,b], Brunno L. Albuquerque[a], Josiel B. Domingos[a,*], Karine Philippot[b,*]

[a]*Chemistry Department (LaCBio), Universidade Federal de Santa Catarina, Florianópolis, SC, C.P. 476, 88040-900, Brazil.*

[b]*CNRS, LCC (Laboratoire de Chimie de Coordination), Université de Toulouse, 205 Route de Narbonne, Toulouse, France.*

*Corresponding authors.

E-mail adresses: josiel.domingos@ufsc.br (J. B. Domingos), karine.philippot@lcc-toulouse.fr (K. Philippot).

Summary

1. Characterization of the nickel nanoparticle samples used as catalysts

1.1. Transmission electron microscopy (TEM) and EDX analysis

TEM observations were carried out at the "Centre de microcaractérisation Raymond Castaing" in Toulouse (UMS-CNRS 3623). TEM grids were prepared by drop-casting of each THF crude colloidal solution onto a holey carbon-coated copper grid followed by drying under vacuum overnight. TEM analyses were performed on a JEOL 1011 electron microscope operating at 100 kV with a resolution point of 4,5 Å. HRTEM observations were carried out with a JEOL JEM 2010 electron microscope working at 200 kV with a resolution point of 2.5 Å and equipped with X-ray analysis PGT (light elements detection, resolution 135 eV) for EDX analysis. Statistical size distributions were built by counting over than 200 non-touching particles with Image J tool software. Origin software was used to get size-distribution histograms fitted to Gaussian or LogNormal functions and determine the mean diameters of the nanoparticles. The mean diameters of the nanoparticles are presented with the standard deviation (sigma) within brackets. The determination of crystalline structure from HRTEM images was performed with Digital Micrograph software.

1.1.1. Ni-OA: Octanoic acid (OA) - stabilized nickel nanoparticles

a) b)

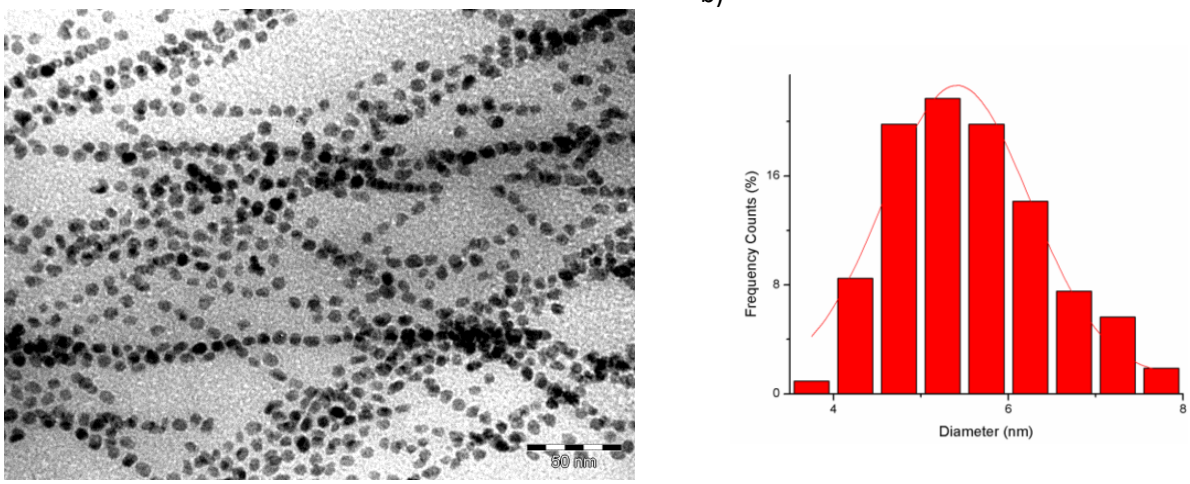

Figure S1 - a) TEM image of Ni-OA nanoparticles. b) Size distribution histogram, d_{mean}= 5.4(1.6) nm.

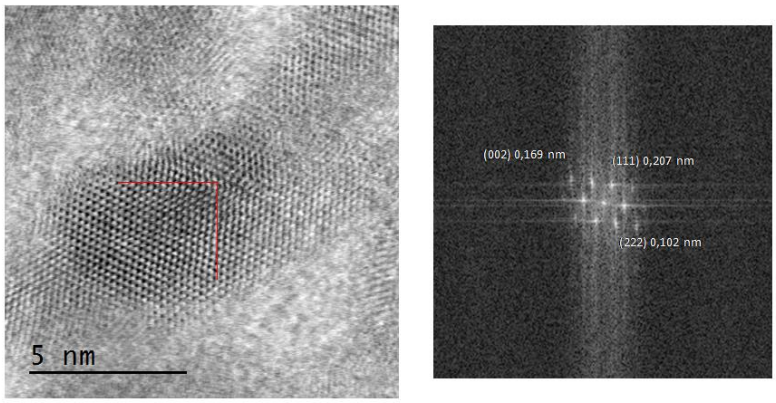

Figure S2 - HRTEM image of Ni-OA nanoparticles before adsorption on the support, and electron diffraction analysis in the [011] direction.

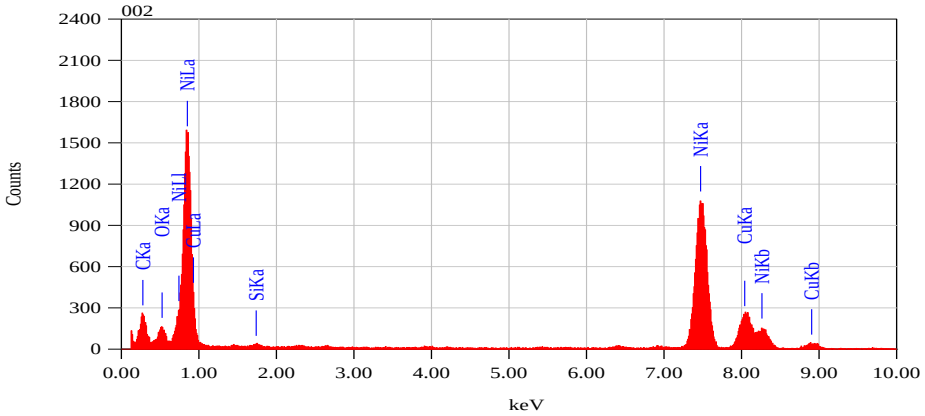

Figure S3 – EDX analysis of Ni-OA nanoparticles.

1.1.2. Ni-OA@SiO_2: Octanoic acid-stabilized nanoparticles after deposition onto silica support

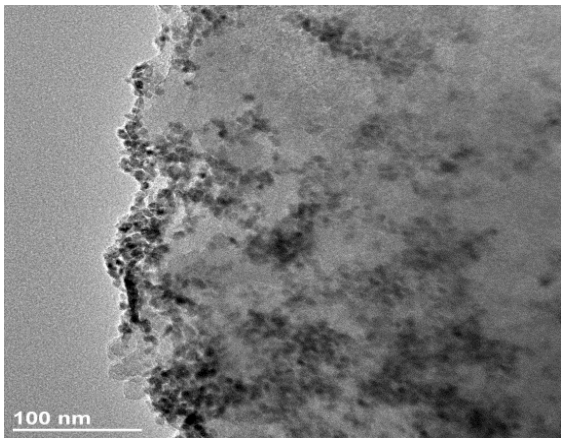

Figure S4 - TEM image of Ni-OA nanoparticles deposited onto SiO_2.

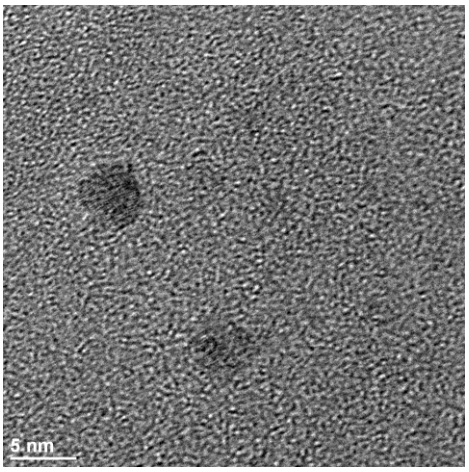

Figure S5 - HRTEM image of isolated Ni-OA@SiO_2 nanoparticles.

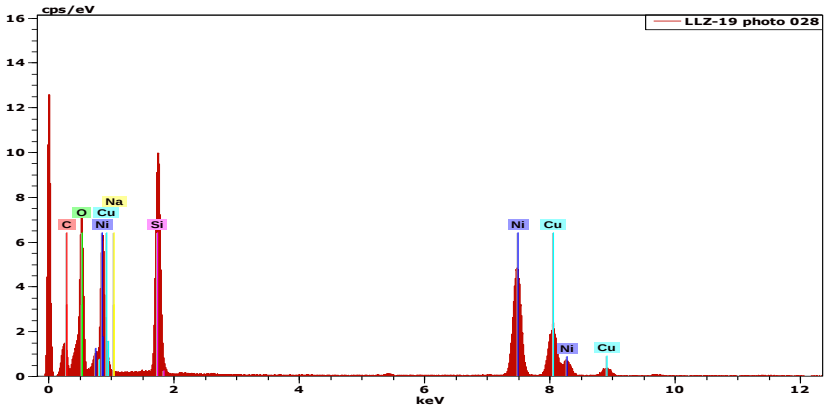

Figure S6 – EDX analysis of Ni-OA@SiO_2 nanoparticles (the peak at 1.8 keV corresponds to silicon from the silica support).

1.1.3. Ni-PVP: polyvinylpyrrolidone (PVP) - stabilized nickel nanoparticles

a)

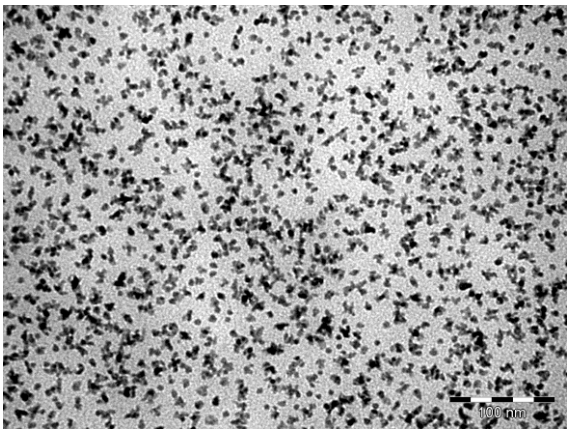

b)

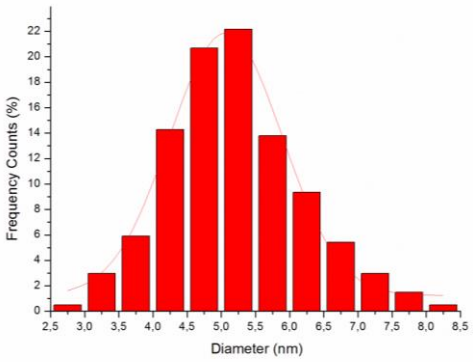

Figure S7- a) TEM image of Ni-PVP nanoparticles. b) Size distribution histogram, d_{mean}= 5.1(1.6) nm.

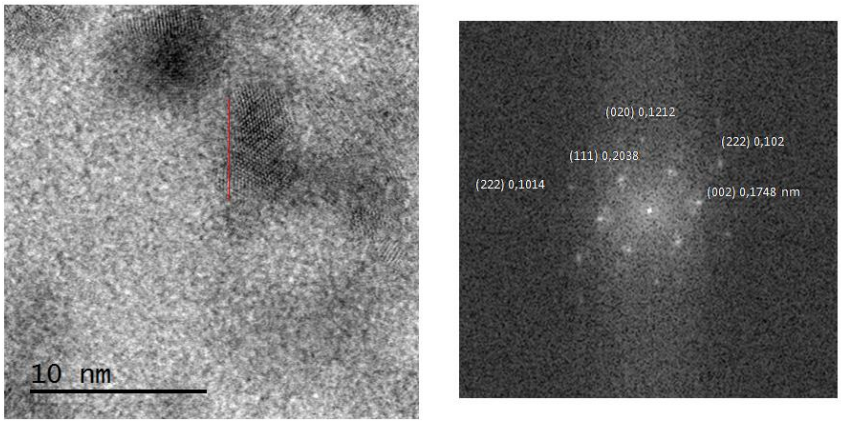

Figure S8 – HRTEM image of Ni-PVP nanoparticles and electron diffraction analysis in the [011] direction.

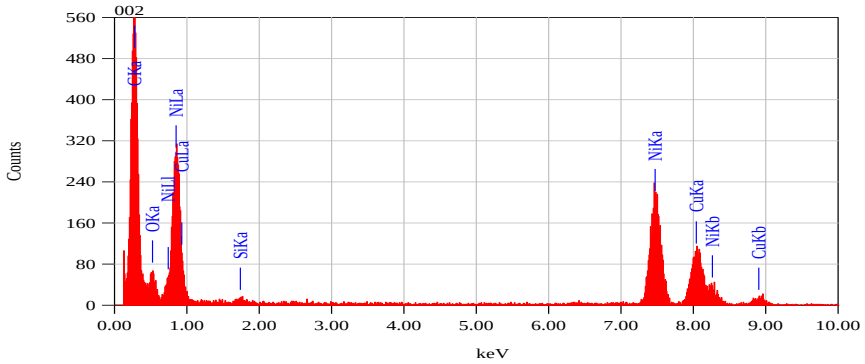

Figure S9 – EDX analysis of Ni-PVP nanoparticles.

1.1.4. Ni-PVP/TPP: polyvinylpyrrolidone-stabilized nickel nanoparticles modified by triphenylphosphine (TPP)

a) b)

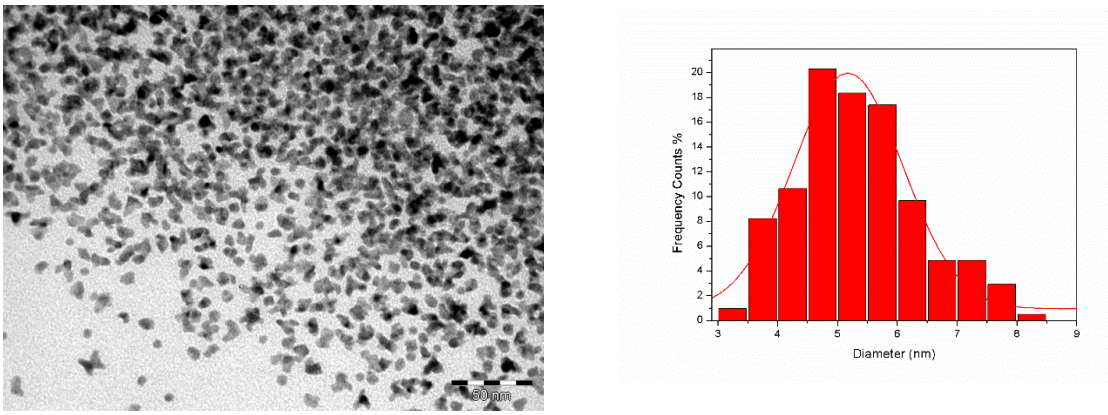

Figure S10 – a) TEM image of Ni-PVP/TPP nanoparticles. b) Size distribution histogram, d_{mean}= 5.2(1.8) nm.

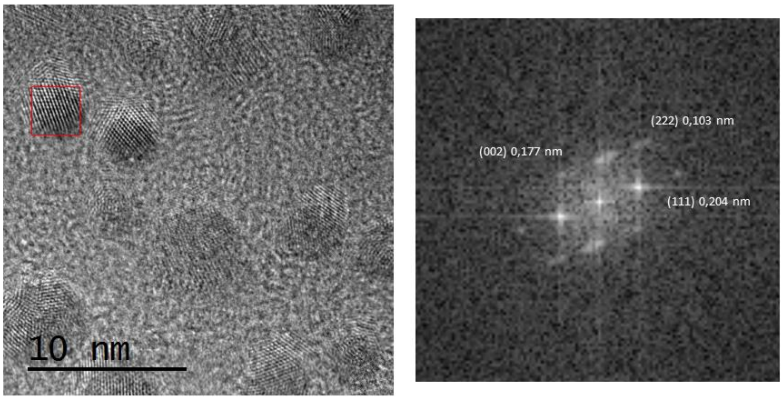

Figure S 11 - HRTEM image of Ni-PVP/TPP nanoparticles and electron diffraction analysis in the [011] direction.

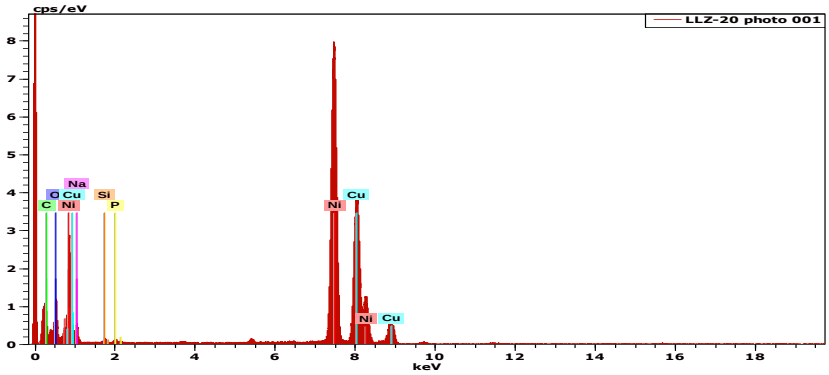

Figure S 12 - EDX analysis of Ni-PVP/TPP nanoparticles.

1.1.5. Ni-SA: Stearic acid (SA) - stabilized nickel nanoparticles

a) b)

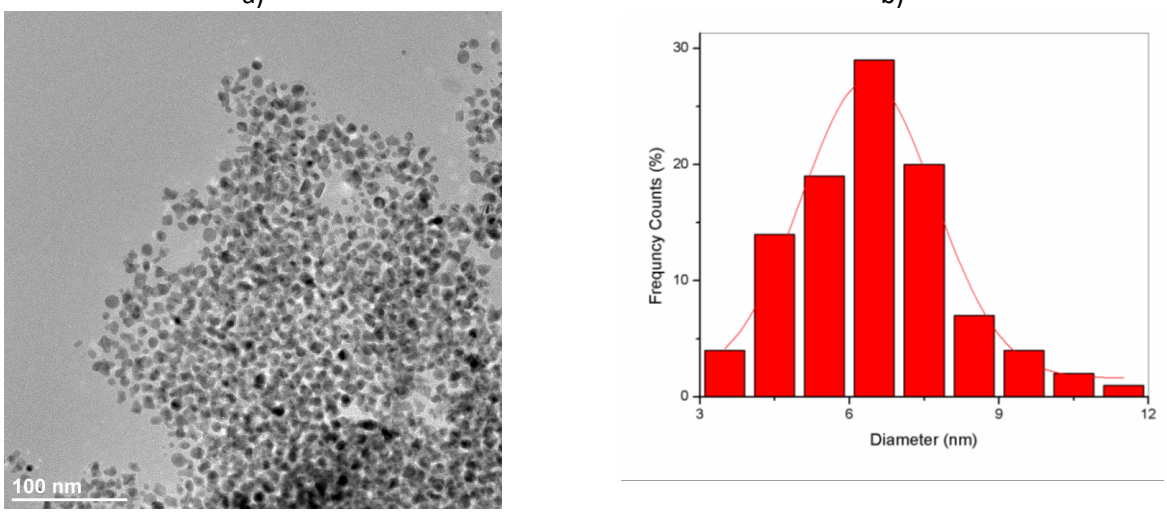

Figure S13 - a) TEM image of Ni-SA nanoparticles. b) Size distribution histogram d_{mean}=6.4(2.6) nm.

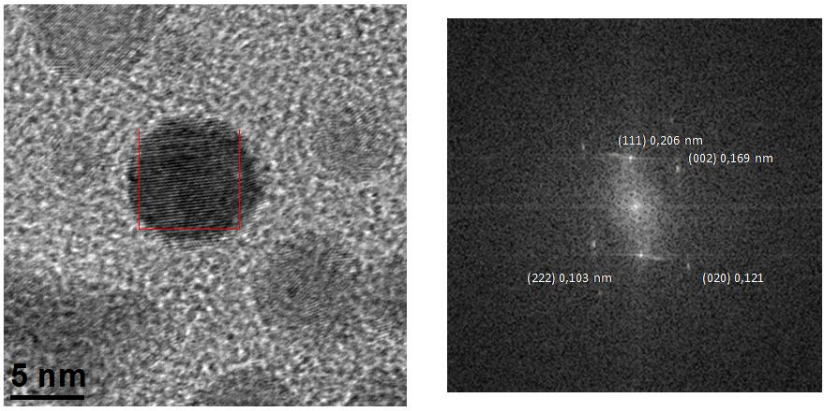

Figure S14 - HRTEM image of Ni-SA nanoparticles and electron diffraction analysis in the [011] direction.

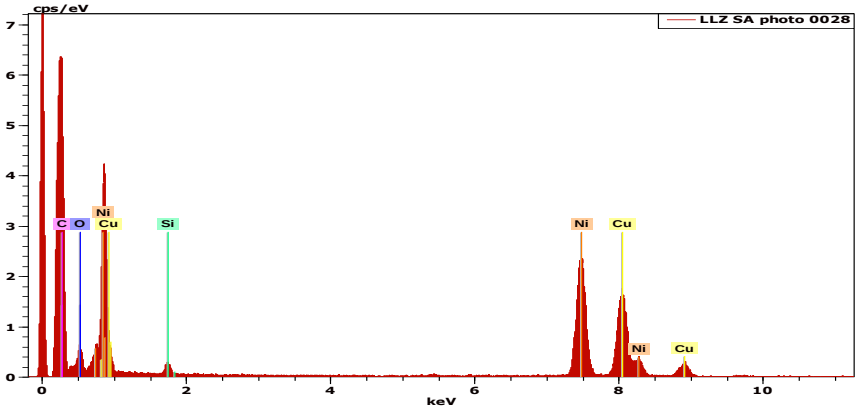

Figure S15 - EDX analysis of Ni-SA nanoparticles

1.1.6. Ni/HDA: Hexadecylamine (HDA) - stabilized nickel nanoparticles

a)

b)

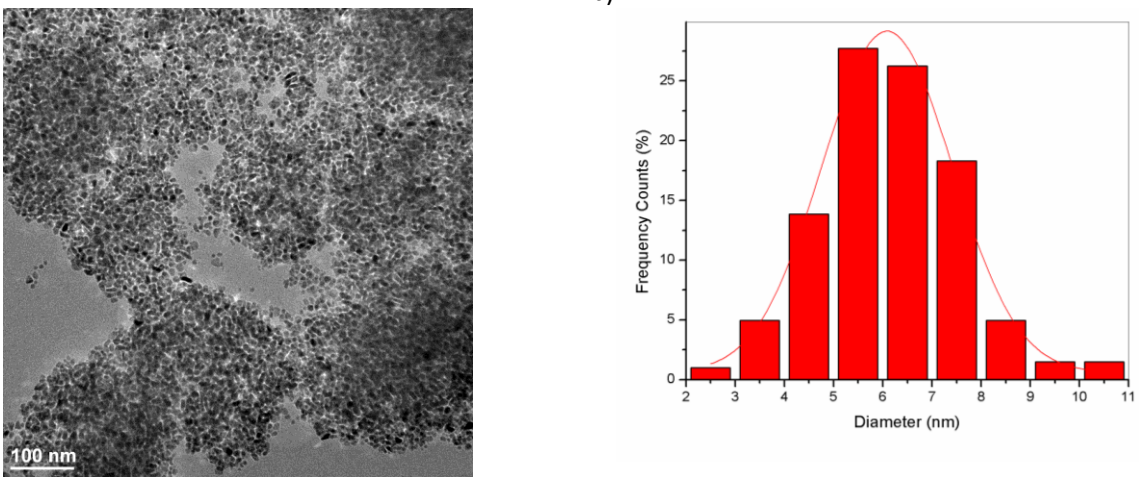

Figure S16 - a) TEM image of Ni-HDA nanoparticles. b) Size distribution histogram, d_{mean}= 6.1(2.6) nm.

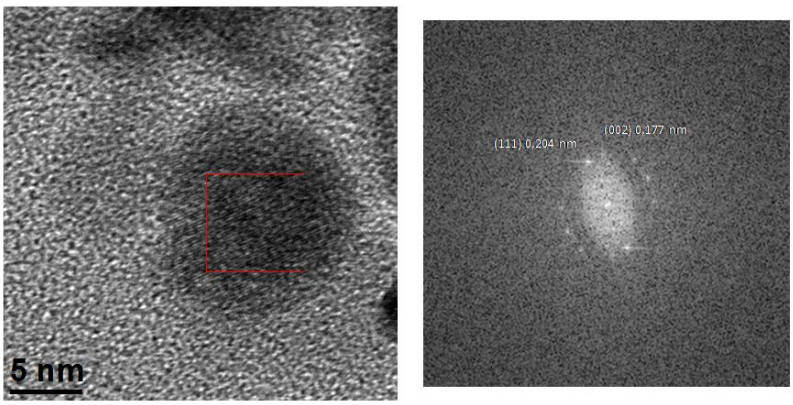

Figure S17 - HRTEM images of Ni-HDA nanoparticles and electron diffraction analysis in the [011] direction.

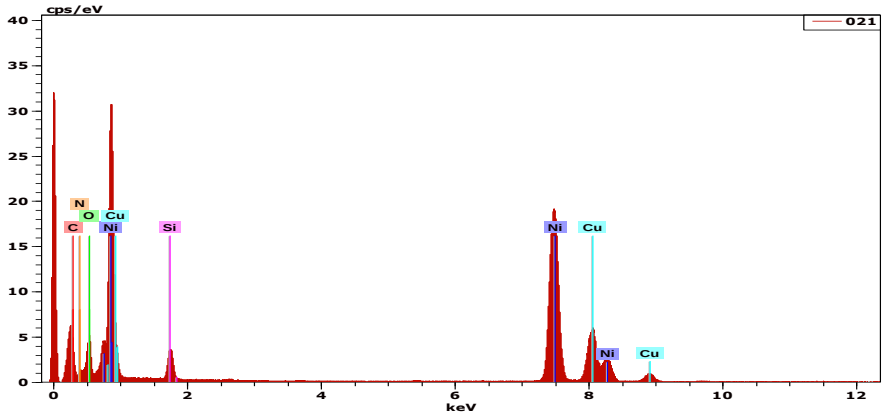

Figure S18 - EDX analysis of Ni-HDA nanoparticles

1.2. Magnetic properties of the nickel nanoparticles determined by SQUID (Superconducting quantum interference device)

The magnetization curves of the nickel nanoparticles were acquired on a Quantum Design Model MPMS 5.5 SQUID magnetometer at the service of magnetic measurements of LCC-CNRS-Toulouse. The saturation magnetization curves were recorded at ± 5 T and 2K. The value of M_s (emu g^{-1}) was calculated from the nickel contents previously determined by ICP-AES analysis. From the M_s value, the magnetic moment (μ_B) was calculated and compared with the bulk nickel. The zero field cooling/ field cooling (ZFC/FC) experiments were performed in the range 2-300K and allowed to get the blockage temperature (T_b).

1.2.1. Ni-OA@SiO_2: Octanoic acid (OA) - stabilized nickel nanoparticles supported into silica

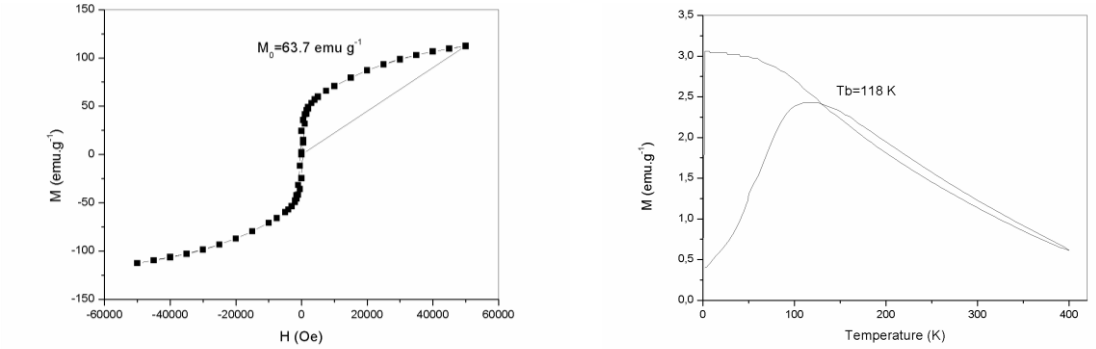

Figure S19 - Saturation magnetization curve for Ni-OA@SiO_2 nanoparticles, M_0=63.7 emu g^{-1} and μ = 0,67 μ_B (left). ZFC/FC susceptibility, T_b=118 K (right).

1.2.2. Ni-PVP: polyvinylpyrrolidone-stabilized nickel nanoparticles

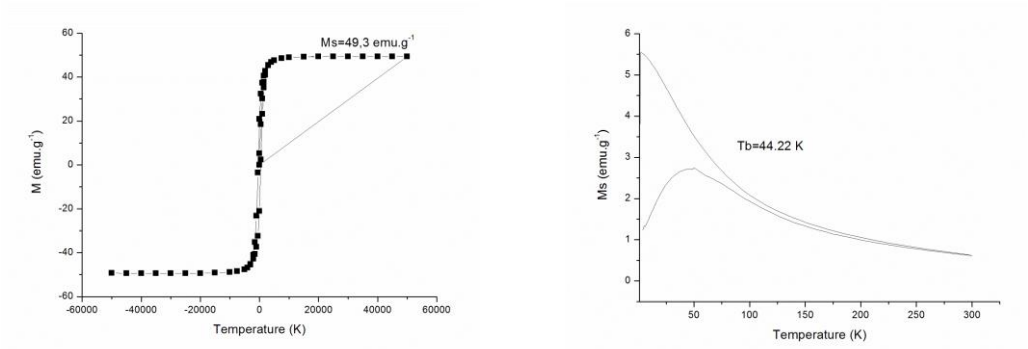

Figure S20 - Saturation magnetization curve for Ni-PVP nanoparticles, M_s=49.3 emu g^{-1} and μ = 0.52 μ_B (left). ZFC/FC susceptibility, T_b=44.2 K (right).

1.2.3. Ni-PVP/TPP: Polyvinylpyrrolidone-stabilized nickel nanoparticles modified by triphenylphosphine (TPP)

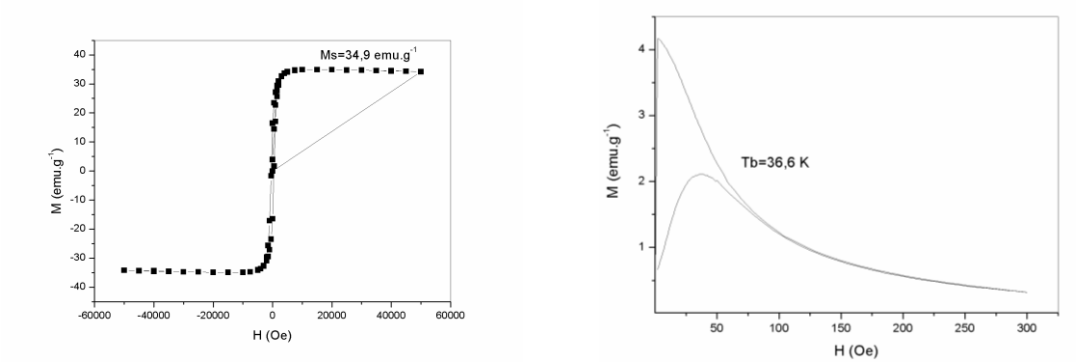

Figure S21 - Saturation magnetization curve for Ni-PVP/TPP nanoparticles, M_s = 34.9 emu g^{-1} and μ = 0.37 μ_B (left). ZFC/FC susceptibility, T_b 36.6 K (right).

1.2.4. Ni-SA: Stearic acid (SA) - stabilized nickel nanoparticles

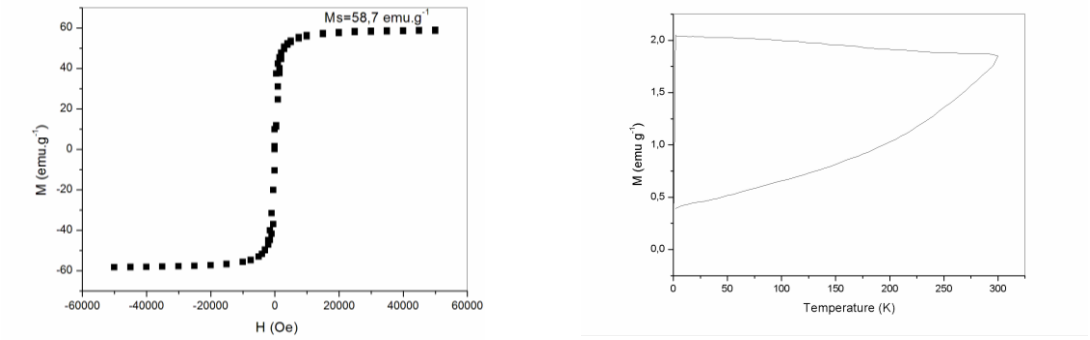

Figure S22 - Saturation magnetization curve for Ni-SA nanoparticles, M_S = 58.7 emu g^{-1} and μ = 0.61 μ_B (left). ZFC/FC susceptibility, T_b could not be detected being up to 300 K (right).

1.2.5. Ni-HDA: Hexadecylamine (HDA) - stabilized nickel nanoparticles

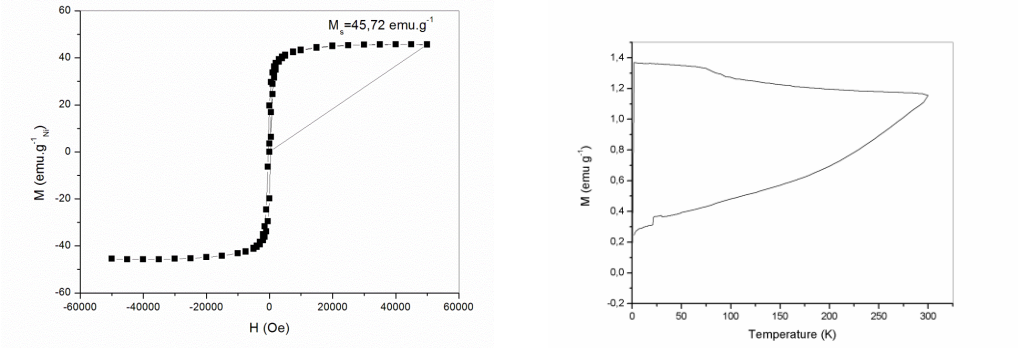

Figure S23 - Saturation magnetization curve for Ni-HDA nanoparticles, Ms = 45.7 emu g^{-1} and μ = 0.48 μ_B (left). ZFC/FC susceptibility, T_b could not be detected, being up to 300K.

1.3. X-Ray Absorption Spectroscopy (XAS) Analysis

The oxidation state of Ni-OA@SiO_2 sample was determined by XAS studies using a Synchrotron based setup. The data were acquired in both the XANES (X-Ray Absorption Near Edge Structure) and EXAFS (Extended X-Ray Absorption Fine Structure) regions. The white line intensity of the *K*-edge XANES spectra is very sensitive to the coordination symmetry and oxidation states of 3d metals. The comparison of Ni-OA@SiO_2 sample data with those of nickel oxide (NiO) and nickel metal (Ni foil) used as references in the XANES region is reported in Figure S26a. This figure clearly shows that the Ni-OA@SiO_2 sample contains Ni(0) species, the pre-edge signal in 8330 eV which is present in Ni foil is also in the Ni-OA@SiO_2 sample is an evidence of reduced Ni species.[2] Fig. S26b corresponds to the graph in *R*-space (without phase correction) obtained after background removal and Fourier Transform application in the EXAFS signal, with comparison of the spectra of the NiO and Ni standards. The great magnitude of the Ni-Ni bond strongly supports that the Ni-OA@SiO_2 sample displays a high quantity of Ni(0) atoms in the nanoparticle. The asymmetry of the Ni-Ni bond peak in the Ni-OA@SiO_2 sample may be due to either the adsorption of the nanoparticles onto the SiO_2 support[3] or the presence of the oleic acid ligand at the metal surface.

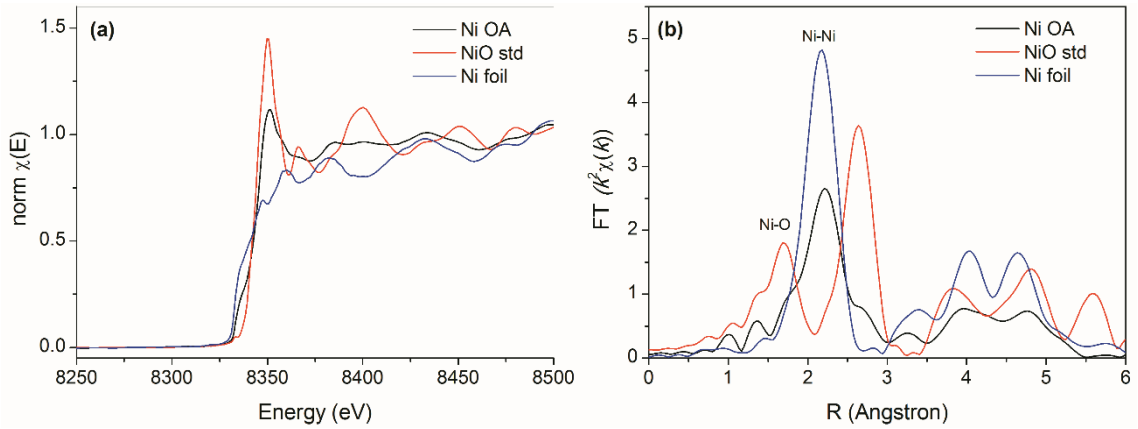

Figure S24. (a) Normalized XANES and (b) Fourier-transformed k^2-weighted EXAFS spectra for the Ni-OA@SiO_2 NPs (black line), the NiO standard (red line) and Ni(0) foil standard (blue line), acquired at room temperature.

The structural parameters of the Ni-OA@SiO_2 sample were obtained by the first-shell fit of the EXAFS signal as shown in Figure S27. The amplitude factor (S_0^2) for the fitting was obtained by the fit of the Ni foil standard using 12 as the average coordination number (N_{Ni-Ni}). As shown in Table S1, the Ni-Ni bond distance, R_{Ni-Ni} obtained for Ni-OA@SiO_2 sample (2.482 Å) is nearly the same as for the Ni foil standard (2.48 Å). The EXAFS Debye-Waller factor, σ^2, calculated for the Ni-OA@SiO_2 sample (0.0088(5)) is larger than the one observed for the Ni foil (0.0055(2)) which indicates a lattice expansion as the result of surface tension and interfacial energy of the Ni-OA nanoparticles.[4] The N_{Ni-Ni} value (10.9(6)) obtained for the Ni-OA@SiO_2 is in agreement with theoretical calculation for cubooctahedron particles[5] and by the integration of a spherical homogeneous model[6] and can be used as a characterization of the nanoparticle size.

Table S1. EXAFS structural parameters obtained by the fit of Ni OA sample. The error in the measurement is indicated in the least significative algarism, ex. 0.0088(5) = 0.0088 ± 0.0005.

Sample	S_0^2	E_0	σ^2	R_{Ni-Ni}	N_{Ni-Ni}	χ_r^2	R-factor
Ni OA	0.7	6.1(8)	0.0088(5)	2.482(1)	10.9(6)	51.86	0.020

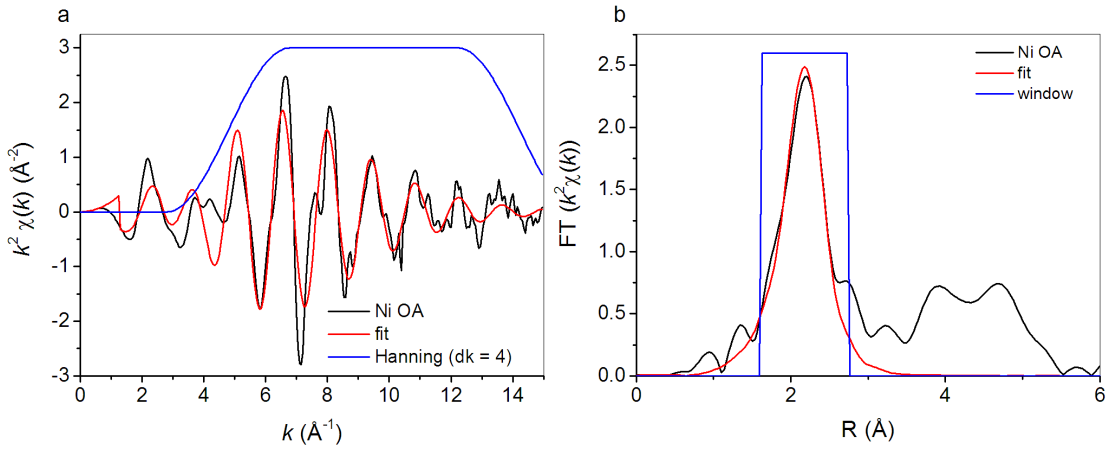

Figure S25. a) k^2-weighted EXAFS and b) Fourier transformed k^2-weighted EXAFS spectra and respective first-shell fit for the Ni OA@SiO_2 sample at room temperature.

2. Complementary data from hydrogenation catalysis studies

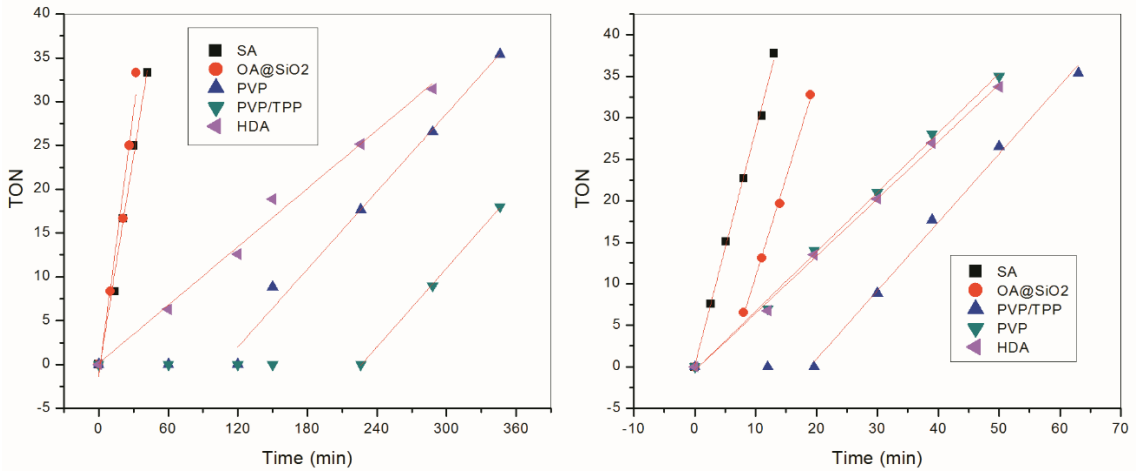

Figure S246 – TON (turn over numbers) as a function of Time for the hydrogenation reaction of *t*-chalcone (left) and styrene (right) with all Ni-NPs catalysts. Reaction conditions: [chalcone] = 0.416 mol L^{-1}, 12.5 µmol Ni, 3 mL of THF, 3 bar H_2, 60 °C.

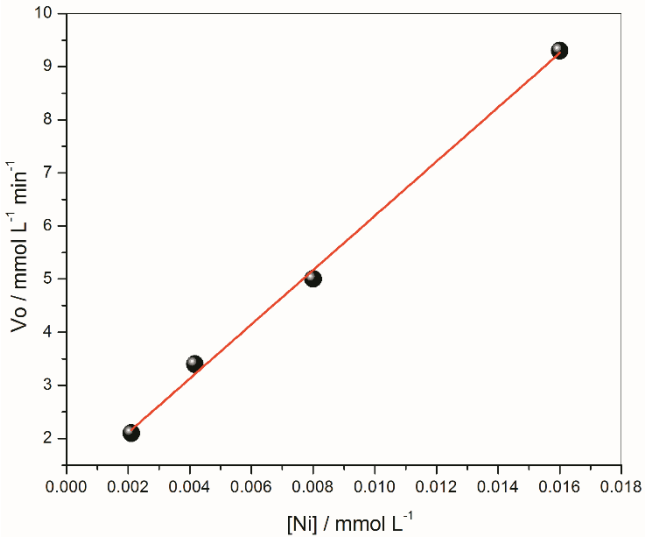

Figure S27 - Log of the initial rate (V_0) as a function of log Ni(0) concentration ([C]) for the hydrogenation reaction of *t*-chalcone by Ni/OA@μ_2 catalyst. Reaction conditions: [*t*-chalcone] = 0.416 mol L^{-1}, 3 bar H_2, 60 °C.

3. Calculation of Nanoparticle Specific Surface Area (*S*)[1]

1) Calculation of the number of metal atoms per nanoparticle (N)

$N = (R_{NP} / R_M)^3$

R_{NP} = Nanoparticle radius
R_M = Metal atom radius

2) Calculation of the volume of one nanoparticle (V_{NP})

$V_{NP} = 4/3\pi \times R_{NP}^3$

3) Calculation of the mass of one nanoparticle (m_{NP})

$m_{NP} = \rho \times V_{NP}$

ρ = bulk metal density

4) Calculation of the mass of nanoparticle in the reaction media (W)

$W = V_R \times M \times AM$

M = Final concentration of metal in the solution
V_R = Final volume of the reaction
AM = Metal atom mass

5) Calculation of the number of formed nanoparticles (N_{NP})

$N_{NP} = W / m_{NP}$

6) Calculation of the total surface area (S_T)

$S_T = (4 \times \pi \times R_{NP}^2 \times N_{NP})$

7) Calculation of the specific surface area (total surface area per unit of volume, *S*)

$S = (4 \times \pi \times R_{NP}^2 \times N_{NP}) / V_R$

4. Recycling study

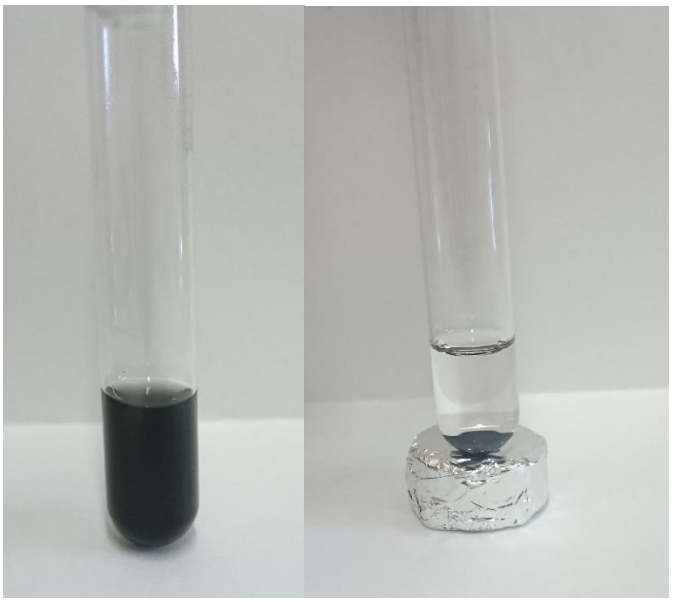

Figure S28 – Pictures of the magnetic recovery of the Ni-OA@SiO_2 catalyst from the reaction media by simple application of a magnet.

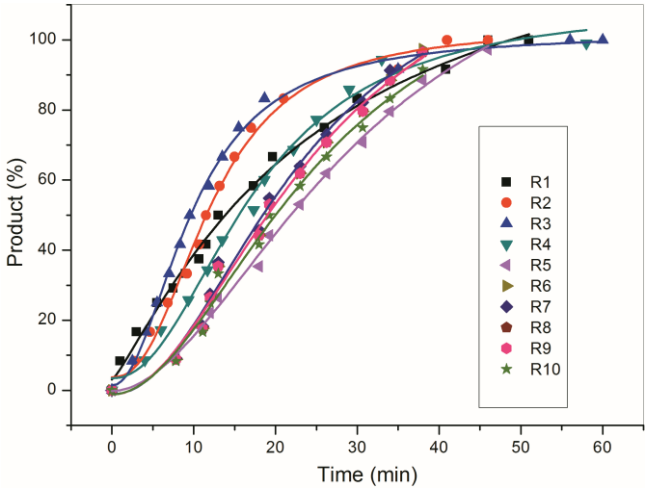

Figure S29 – Product conversion as a function of Time for the hydrogenation reaction of *t*-chalcone in 10 recycling times with the Ni-OA@SiO_2 catalyst. Reaction conditions: [chalcone] = 0.416 mol L^{-1}, 62.5 µmol Ni, 3 mL of THF, 4 bar H_2, 60 °C.

a) b)

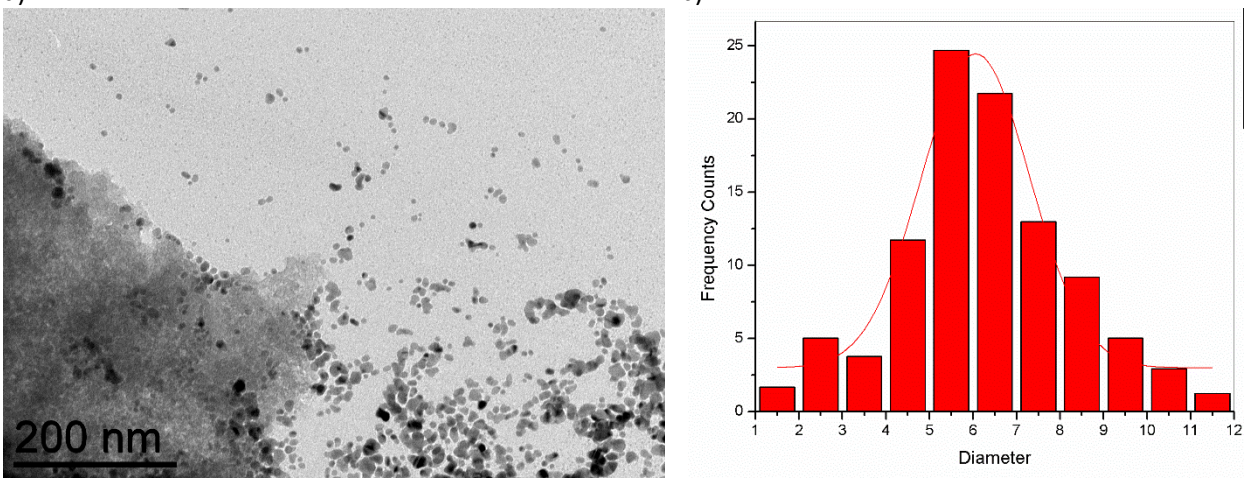

Figure S30 - TEM image of Ni-OA@SiO_2 nanoparticles after reaction. b) Size distribution histogram, d_{mean}= 6.1(2.6) nm.

5. References

1. W. C. Elias, R. Eising, T. R. Silva, B. L. Albuquerque, E. Martendal, L. Meier and J. B. Domingos, *The Journal of Physical Chemistry C*, 2014, **118**, 12962-12971.
2. T. A. Maia and E. M. Assaf, *Rsc Advances*, 2014, **4**, 31142-31154.
3. X. Yang, D. Chen, S. Liao, H. Song, Y. Li, Z. Fu and Y. Su, *Journal of Catalysis*, 2012, **291**, 36-43.
4. Z. Wei, T. Xia, J. Ma, W. Feng, J. Dai, Q. Wang and P. Yan, *Materials Characterization*, 2007, **58**, 1019-1024.
5. A. Jentys, *Physical Chemistry Chemical Physics*, 1999, **1**, 4059-4063.
6. S. Calvin, M. M. Miller, R. Goswami, S.-F. Cheng, S. P. Mulvaney, L. J. Whitman and V. G. Harris, *Journal of Applied Physics*, 2003, **94**, 778-783.